

A Compact Broadband Circularly-Polarized Patch Antenna with Wide Axial-Ratio Beamwidth for Universal UHF RFID Applications

Zhongbao Wang^{*}, Ya-Nan Wang, Xinhong Liu, Hongmei Liu, and Shaojun Fang

Abstract—A compact broadband circularly-polarized (CP) patch antenna with a wide 3-dB axial-ratio (AR) beamwidth is proposed for universal ultra-high-frequency (UHF) radio frequency identification (RFID) applications. The proposed antenna consists of four triangular radiation patches and a compact feed network. Each of the radiation patches is grounded by shorting pins for 3-dB AR beamwidth enhancement and patch miniaturization. The feed network having a miniaturized hybrid coupler and two trans-directional couplers is proposed for good circular polarization. Measured results show that the -10 -dB impedance bandwidth of the antenna is 18.4% (820–986 MHz); the 2.5-dB AR bandwidth is 32.8% (700–975 MHz); and the gain is 5.12 dBic. The measured 3-dB AR beamwidths for the planes of $\phi = 0^\circ$ and $\phi = 45^\circ$ are 177° and 190° , respectively. The overall antenna size is $0.408\lambda_0 \times 0.408\lambda_0 \times 0.053\lambda_0$ at 900 MHz.

1. INTRODUCTION

Radio frequency identification (RFID) is developing extensively and is driving Industry 4.0 revolution [1]. Owing to the fast reading rate and long-distance battery-less reading capability, ultra-high-frequency (UHF) RFID has been widely used in logistics management, smart tracking, electronic toll collection, store security, and other fields through non-contact automatic identification of radio frequency signals. The UHF RFID reader antenna is a key element to maximize reading range. However, the UHF frequencies authorized for RFID applications are different in different countries and regions. Therefore, the design of a compact broadband antenna having a bandwidth larger than 12.8% (840–955 MHz) is of great significance to cover all UHF RFID operation bands.

In general, RFID tag antennas are linear polarization. Considering the arbitrary orientation of the tags, circularly-polarized (CP) antennas are usually used in UHF RFID readers to avoid polarization mismatch and enable tag reading [2]. So far, many CP patch antennas have been presented for UHF RFID reader applications. There are two types of CP patch antennas, including a multi-feed version and a single-feed version. However, the single-feed single-patch CP antennas have inherently narrow impedance and axial ratio (AR) bandwidths [3]. In [4], the CP antenna has impedance and AR bandwidths of less than 2%. To achieve wide impedance and AR bandwidths, some techniques have been proposed, including the use of parasitic patches [5], L-shaped ground plane [6], coupled rotated vertical metallic plates [7, 8], and a stacked structure [2, 9]. In [5], a CP patch antenna was achieved by using an eccentric annular patch and a parasitic element loaded beside the radiating patch. The impedance bandwidth was enhanced to be 56.5%, but the AR bandwidth was only 6.13%. Based on a direct-feed single-layer corner-truncated square patch antenna with an L-shaped ground plane, a novel technique of loading three narrow slits into the corner-truncated square patch was proposed in [6]. Broad impedance and AR bandwidth of 48.6% and 16.4%, respectively, were attained. However, the height of the CP patch antennas [5, 6] was larger than $0.17\lambda_0$. In [7], a stacked structure using a modified half

Received 27 March 2021, Accepted 14 May 2021, Scheduled 18 May 2021

^{*} Corresponding author: Zhongbao Wang (wangzb@dlmu.edu.cn).

The authors are with the School of Information Science and Technology, Dalian Maritime University, Dalian, Liaoning 116026, China.

E-shaped patch, a parasitic patch, and four rotated vertical metallic plates on the ground plane was presented, which had the impedance and AR bandwidths of 14.2% and 9.0%, respectively. However, the structure of the CP patch antenna [7] is very complex, and the AR bandwidth is still narrow, which cannot cover all UHF RFID operation bands.

Compared to the single-feed version, multi-feed CP patch antennas have better impedance and AR bandwidths [10–13]. In [10], a 3-dB T-type power divider with a 90° phase-shifting line was arranged at the inside of the annular-ring patch for producing CP radiation, and a circular parasitic patch was suspended above the annular ring, which had the impedance and AR bandwidths of 10.6% and 6.0%, respectively. In [11], a stacked patch antenna fed by a 3-dB branch-line coupler enhanced the AR bandwidth to 17.7%. However, the used three layers of patches resulted in an antenna height of larger than $0.074\lambda_0$. Furthermore, three or four feeds of the patch were sequentially connected to the microstrip line and spatially positioned to achieve 90° phase differences between two adjacent feed points, and 3-dB AR bandwidths of 10.7% and 16.4% have been achieved, respectively [12, 13]. However, these CP antennas have narrow 3-dB AR beamwidth.

Many works have been done to design compact CP patch antennas for UHF RFID readers. By etching a cross-slot in the radiation patch and loading four grounded coupling patches on the four corners of the radiation patch, the antenna size was reduced to $0.36\lambda_0 \times 0.36\lambda_0 \times 0.05\lambda_0$ [14]. The realized gain at 922 MHz was 5.5 dBic with an AR bandwidth of 4.9%. In [15], a low-profile CP annular-ring patch antenna with the height of $0.032\lambda_0$ was proposed, which had the impedance and AR bandwidths of 3.5% and 0.65%, respectively. Besides, meta-surfaces were used to reduce the height of CP patch antennas [16] and generate CP radiation [17, 18]. However, this method is complicated. The bandwidth and 3-dB AR beamwidth of these CP antennas [14–16] are narrow.

To provide wide angular coverage, it is critical for a CP RFID antenna to have a wide 3-dB AR beamwidth. In [4], asymmetric-circular-shaped slotted CP patch antennas with slits were proposed for RFID applications, which had a 3-dB AR beamwidth of 100°. In [19], a 3-dB AR beamwidth of 121° was achieved by dielectric loading of a vertical elliptical-patch antenna. In [20], the 3-dB AR beamwidth of a probe-feed square patch antenna was extended to 140° by using the pin-loaded technique. In [21], by etching two pairs of asymmetric slots on the patch and loading coupled strips, a 3-dB AR beamwidth of 188° was obtained. Up to now, most of the AR beamwidth enhancement methods have been proposed for satellite communications or GPS applications [19–21], whose the AR bandwidth is narrow (less than 3.5%).

In this paper, a compact broadband CP patch antenna with a wide 3-dB AR beamwidth is proposed for universal UHF RFID applications. The antenna consists of four triangular radiation patches and a compact feed network. Each of the radiation patches is grounded by shorting pins and fed with phase angles of 0°, -90°, -180°, and -270°, respectively. The shorting pins not only effectively reduce the antenna size but also increase the 3-dB AR beamwidth. Furthermore, a compact feed network having a miniaturized 3-dB hybrid ring coupler and two 3-dB trans-directional (TRD) couplers [22] is proposed for good circular polarization.

2. ANTENNA DESIGN AND PARAMETRIC STUDIES

Figure 1 shows the configuration of the proposed compact broadband CP patch antenna with a wide 3-dB AR beamwidth, which consists of four triangular radiation patches and a compact feed network. Each of the radiation patches having a circular defect structure is fed by a coplanar circular coupling patch with a probe and grounded by the shorting pins. The radiation patches and circular coupling patches are printed on the top side of an FR4 substrate with the thickness $h_1 = 1.6$ mm, dielectric constant $\epsilon_{r1} = 4.4$, and loss tangent $\tan \delta_1 = 0.02$. The feed network is implemented on an F4B substrate with the thickness $h_2 = 1.0$ mm, dielectric constant $\epsilon_{r2} = 2.73$, and loss tangent $\tan \delta_2 = 0.003$. An air gap with a height of $h = 15$ mm between the substrates is used to broaden the bandwidth. Note that the substrates have a dimension of $136 \text{ mm} \times 136 \text{ mm}$ ($L_s \times L_s$). Figure 2 shows the details of the radiation patch and circular coupling patch. Each of the radiation patches is an isosceles right triangle with a hypotenuse length of $L_p = 128$ mm, which is connected to the ground plane by the shorting pins with a diameter of $D_s = 1.0$ mm. The gap-width between the triangular radiation patches is $G = 8$ mm. The distance between the shorting pin and the hypotenuse of the triangular radiation

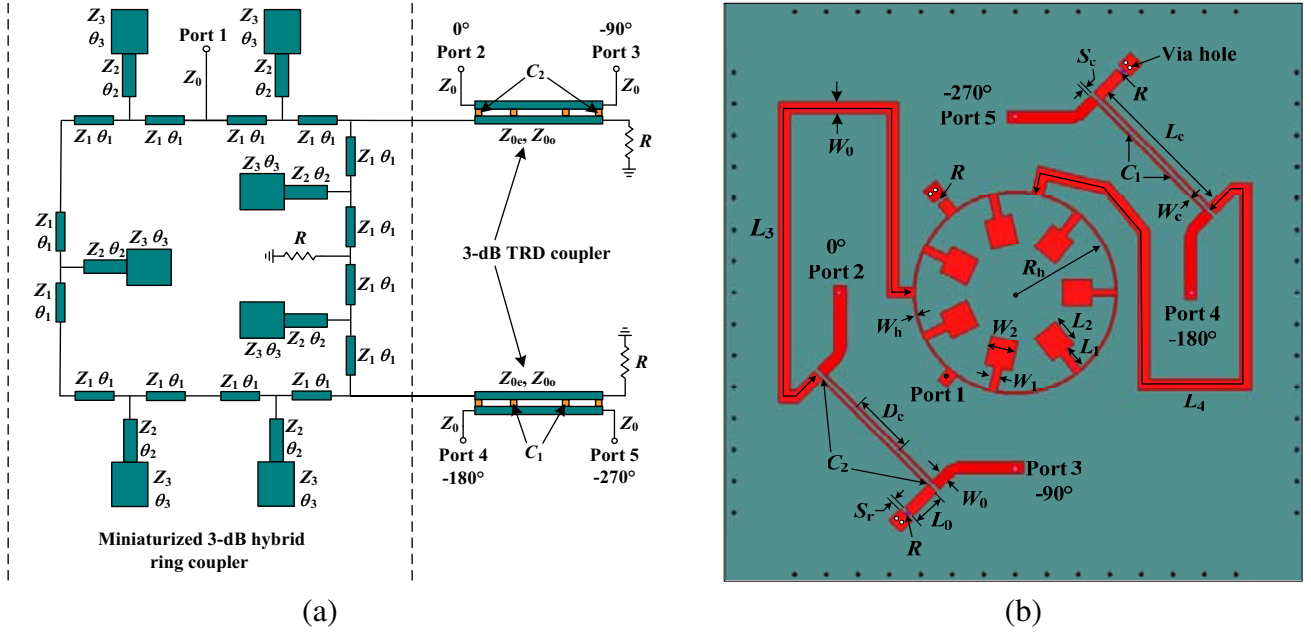


Figure 4. Configuration of the proposed feed network. (a) Equivalent circuit. (b) Layout ($W_0 = 2.8$ mm, $W_1 = 2.0$ mm, $W_2 = 6.0$ mm, $W_c = 1.0$ mm, $W_h = 0.5$ mm, $R_h = 23.5$ mm, $L_0 = 7.8$ mm, $L_1 = 5.5$ mm, $L_2 = 7.2$ mm, $L_3 = L_4 = 155.6$ mm, $L_c = 33.7$ mm, $S_c = 1.0$ mm, $S_r = 1.0$ mm, $D_c = 14.1$ mm, $C_1 = 5$ pF, $C_2 = 3$ pF, $R = 51 \Omega$).

the shorting pins. By using the shorting pins, the 3-dB AR beamwidth is increased from 109° to 173° .

Figure 4 shows the configuration of the proposed feed network, which is composed of a miniaturized 3-dB hybrid ring coupler and two identical 3-dB TRD couplers. The 3-dB hybrid ring coupler provides equal-power anti-phase outputs. For miniaturization, each of the $\lambda/6$ uniform transmission-line sections in the $7\lambda/6$ ring coupler [23] is replaced by a T-type structure. The T-type structure is composed of two-section transmission lines (Z_1 , θ_1) and a step-impedance open-circuited stub (Z_2 , θ_2 , and Z_3 , θ_3), as shown in Figure 4(a). Based on the equivalent theory [24], the design equations of the miniaturized 3-dB hybrid ring coupler are derived as follows,

$$Z_1 = \frac{Z_h \sin \theta_h}{\tan \theta_1 (1 + \cos \theta_h)}, \quad (1)$$

$$\frac{Z_2 Z_3 \cot \theta_3 - Z_2^2 \tan \theta_2}{Z_2 + Z_3 \cot \theta_3 \tan \theta_2} = \frac{Z_h \sin \theta_h \cos^2 \theta_1}{\sin^2 \theta_h - 4 \sin^2 \theta_1 \cos^2 \frac{\theta_h}{2}}, \quad (2)$$

$$Z_h = Z_0 \sqrt{3 - \frac{1}{2} \left(\cot^2 \frac{\theta_h}{2} + \tan^2 \frac{\theta_h}{2} \right)}, \quad (3)$$

where Z_h and θ_h are the characteristic impedance and electrical length of the $\lambda/6$ uniform transmission lines in the $7\lambda/6$ ring coupler [23], respectively. Z_0 is the port impedance. The solution of Equations (1)–(3) is not unique, which implies that four variables (e.g., θ_1 , θ_2 , θ_3 , and Z_3) can be used to flexibly design the miniaturized 3-dB hybrid ring coupler. The 3-dB TRD coupler is composed of a set of coupled microstrip lines and four loading capacitors [22], which can provide a balanced output power distribution and 90° phase difference between output ports 2 and 3 (meanwhile, 90° phase difference between output ports 4 and 5), as shown in Figure 4(a). Based on the theoretical analysis and calculation of the TRD coupler [22], the loading capacitors (C_1 , C_2) and the electrical parameters of the coupled lines (Z_{0e} , Z_{0o} , θ) can be obtained. Then, the physical dimensions of the transmission lines can be calculated by using the transmission-line synthesis tool ADS *Linecalc*. After the HFSS EM simulation, the layout and dimensions of the proposed feed network are obtained and shown in Figure 4. Port 1

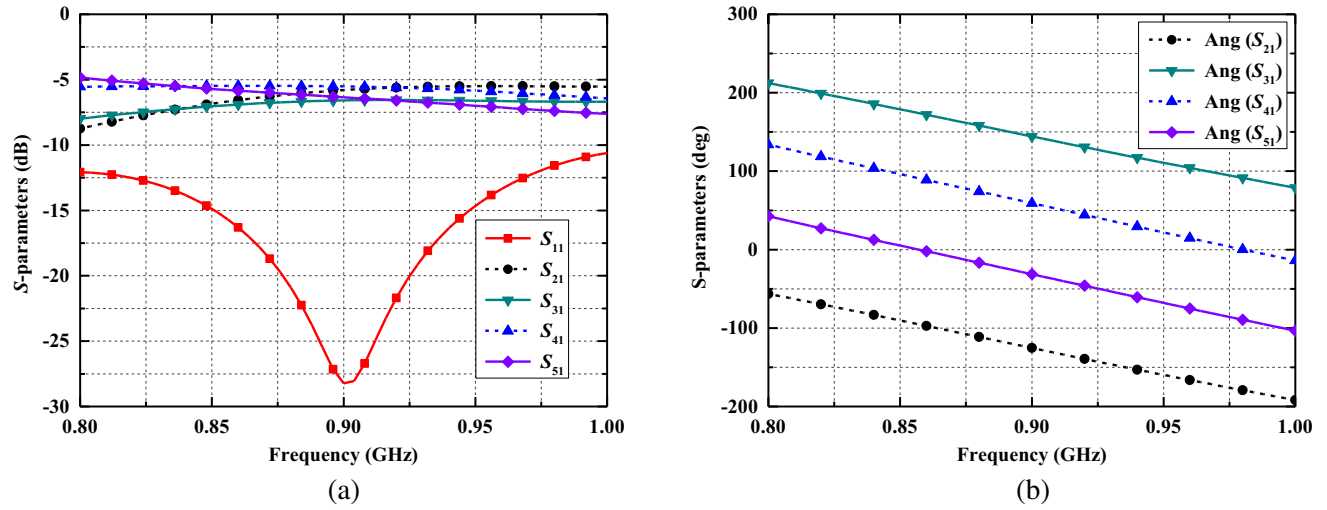


Figure 5. Simulated S -parameters of the proposed feed network. (a) Amplitude. (b) Phase.

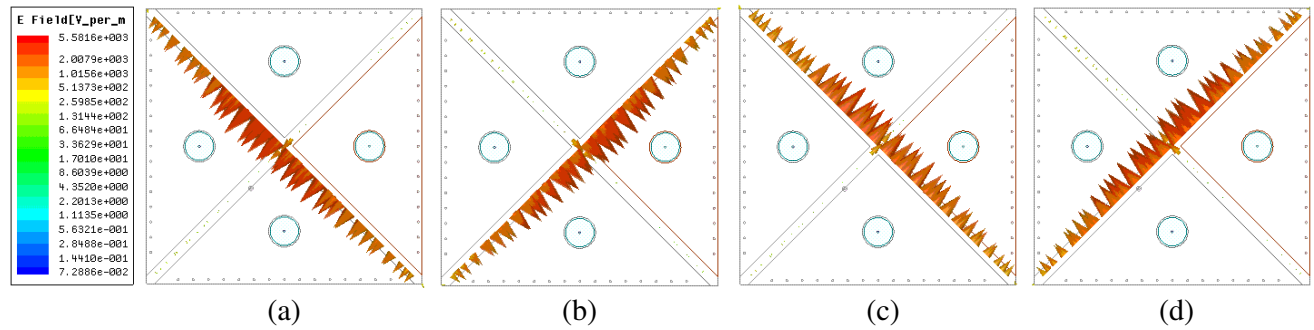


Figure 6. Simulated electric field vector distribution in the slots between the triangular patches at different time instants. (a) $\omega t = 0$. (b) $\omega t = \pi/2$. (c) $\omega t = \pi$. (d) $\omega t = 3\pi/2$.

is the input port of the feed network. The anti-phase output ports of the miniaturized 3-dB hybrid ring coupler are connected to the input ports of the TRD couplers by two equal-length $50\text{-}\Omega$ microstrip lines ($L_3 = L_4$). The simulated S -parameters of the proposed feed network are shown in Figure 5. It is seen that the proposed feed network has a balanced power distribution between the output ports (6.3 ± 0.8 dB) from 840 MHz to 960 MHz with $|S_{11}| < -13$ dB. The phase difference between adjacent output ports is $90^\circ \pm 7^\circ$.

Figure 6 gives the time-varying electric field vector distribution in the slots between the triangular patches at the center frequency of $f_0 = 900$ MHz. It is observed at different instantaneous times $\omega t = 0, \pi/2, \pi$, and $3\pi/2$, where $\omega = 2\pi f_0$ is the angular frequency. The magnitudes of electric field vector distributions at $\omega t = 0$ and π are almost the same, while their directions are opposite. The electric field rotating direction shown in Figure 6 is anticlockwise, leading to a right-handed circularly-polarized (RHCP) radiation.

Figure 7 gives the effect of the height of the air gap h on $|S_{11}|$ and AR of the proposed CP patch antenna. It is observed that the height of the air gap h has a significant effect on the $|S_{11}|$ and AR of the antenna. When h is increased from 10 to 20 mm, both the frequencies for minimum $|S_{11}|$ and AR are decreased, especially for AR. This is because the resonant frequency of the triangular radiation patch shifts down as the air gap increases. Figure 8 gives the effect of the gap-width G between the triangular radiation patches on $|S_{11}|$ and AR of the proposed CP patch antenna. When the gap-width G is increased from 6 to 10 mm, the impedance bandwidth is slightly increased, and the AR in the upper band is improved, but the AR in the lower band (near 840 MHz) is degraded. Thus, the gap-width

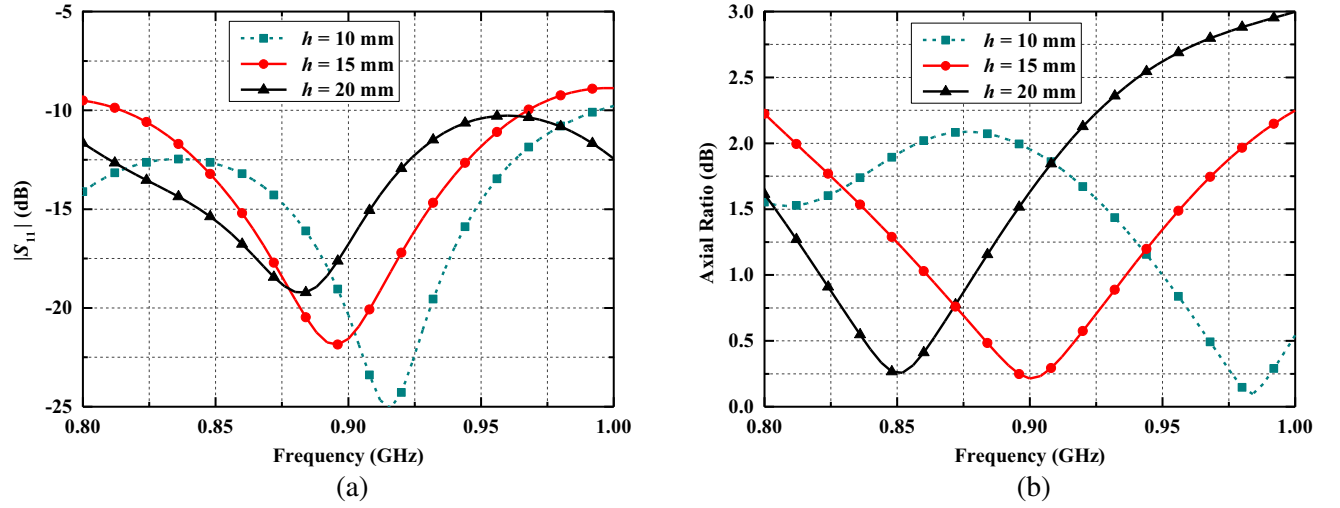


Figure 7. Effect of the air-gap height h on the performances of the proposed CP patch antenna. (a) $|S_{11}|$. (b) AR.

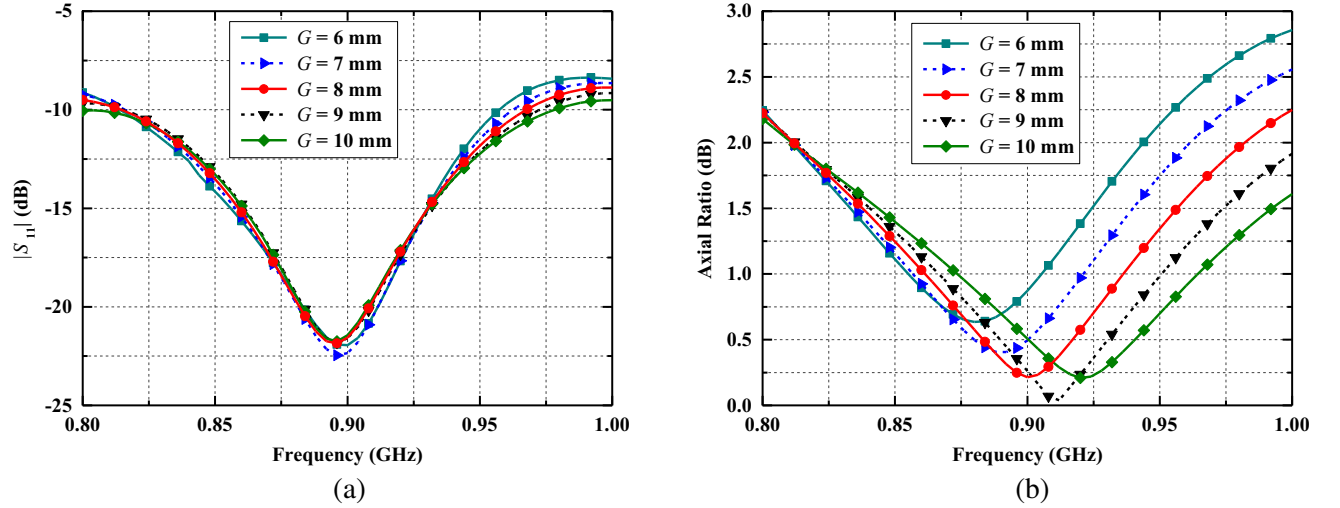


Figure 8. Effect of the gap-width G between the triangular radiation patches on the performances of the proposed CP patch antenna. (a) $|S_{11}|$. (b) AR.

$G = 8$ mm is selected as a compromise between the AR and impedance matching in the band from 840 to 955 MHz for universal UHF RFID applications.

Figures 9 and 10 give the effect of the slot-width S between the circular coupling patch and the triangular radiation patch on $|S_{11}|$, AR, and gain of the proposed CP patch antenna. When the slot-width S is increased from 0.2 to 1.4 mm, $|S_{11}|$ at 900 MHz is improved, but the antenna gain is decreased. This is because the reflection wave from the circular coupling patch and triangular radiation patch is increased and absorbed by three resistors R in the feed network. Besides, the AR is degraded when the slot-width S is changed from 0.8 to 0.2 or 1.4 mm. Figures 11 and 12 give the effect of the number of the shorting pins n on gain, $|S_{11}|$, and AR of the proposed CP patch antenna. When the number of the shorting pins n is increased from 5 to 15, the antenna gain is increased, and the AR in the upper band is improved. For n greater than 15, the effect of the shorting pins on gain, $|S_{11}|$, and AR is slight. Thus, the number of the shorting pins $n = 15$ is selected as a compromise between manufacturing complexity and antenna performances.

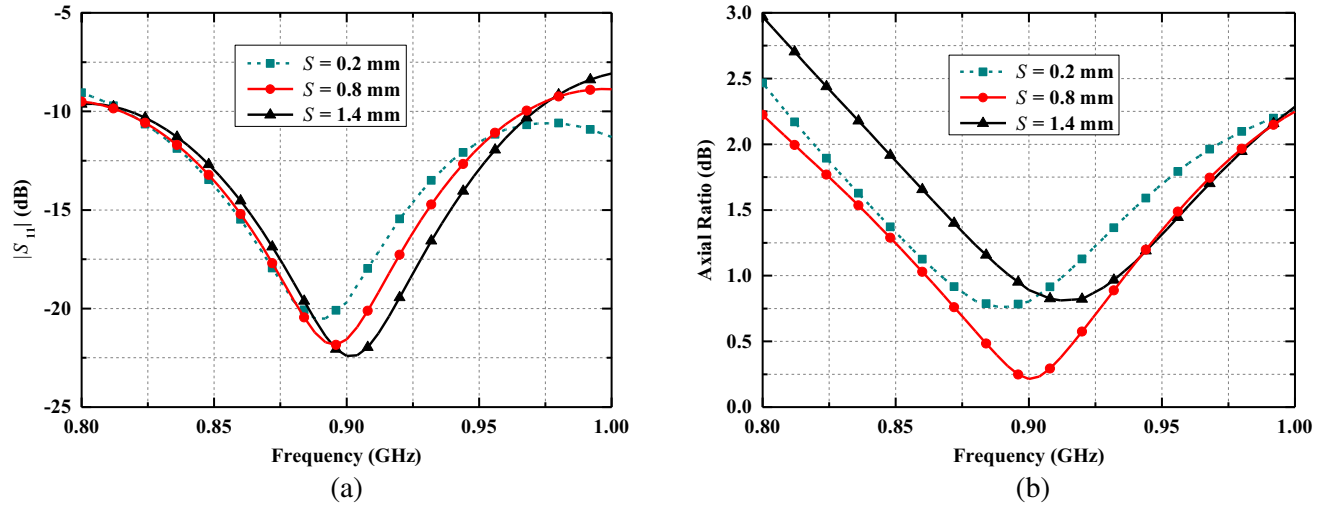


Figure 9. Effect of the slot-width S between the circular coupling patch and the triangular radiation patch on the performances of the proposed CP patch antenna. (a) $|S_{11}|$. (b) AR.

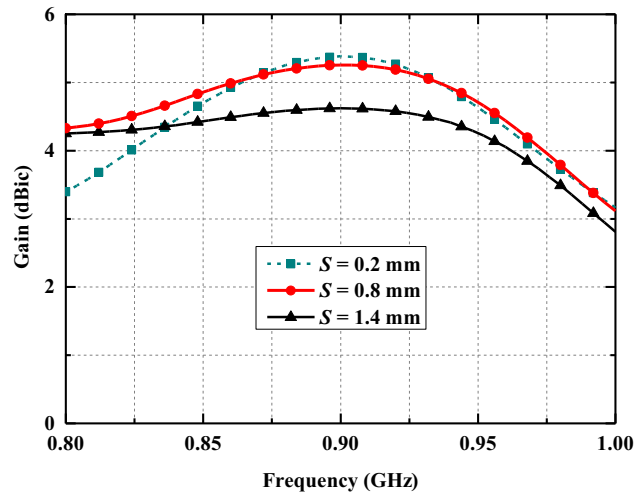


Figure 10. Effect of the slot-width S between the circular coupling patch and the triangular radiation patch on the gain of the proposed CP patch antenna.

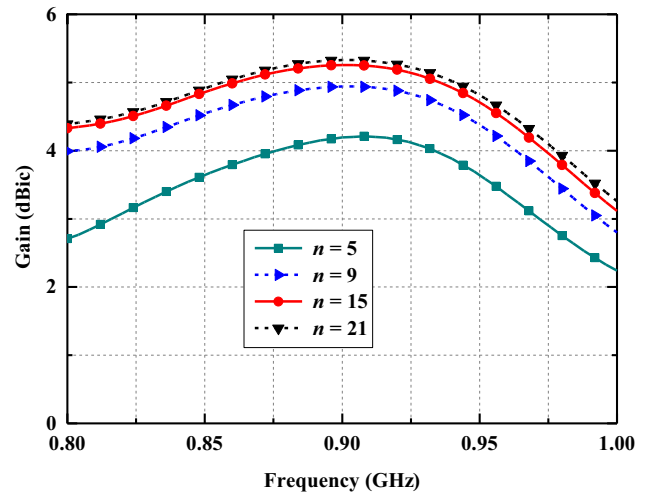


Figure 11. Effect of the number of the shorting pins n on the gain of the proposed CP patch antenna with $(n - 1)D = 105$ mm.

3. EXPERIMENTAL RESULTS AND DISCUSSIONS

The prototype of the proposed CP antenna is fabricated and shown in Figure 13. The far-field performances of the fabricated antenna are measured in an anechoic chamber, and the S -parameters are measured by an Agilent N5230A vector network analyzer.

Figure 14(a) gives the simulated and measured $|S_{11}|$ of the proposed CP antenna. The measured $|S_{11}|$ is less than -10 dB from 820 to 986 MHz (18.4%), which can easily cover the entire UHF RFID band (840–955 MHz). Figure 14(b) gives the AR and gain at boresight. The measured AR bandwidths are less than 2.5 dB from 700 to 975 MHz (32.8%). In the universal UHF RFID bands, the measured AR is less than 2 dB, and the gain is more than 4.3 dBic with a peak gain of 5.12 dBic. There are some discrepancies between the simulated and measured results, which are mainly due to inaccurate values

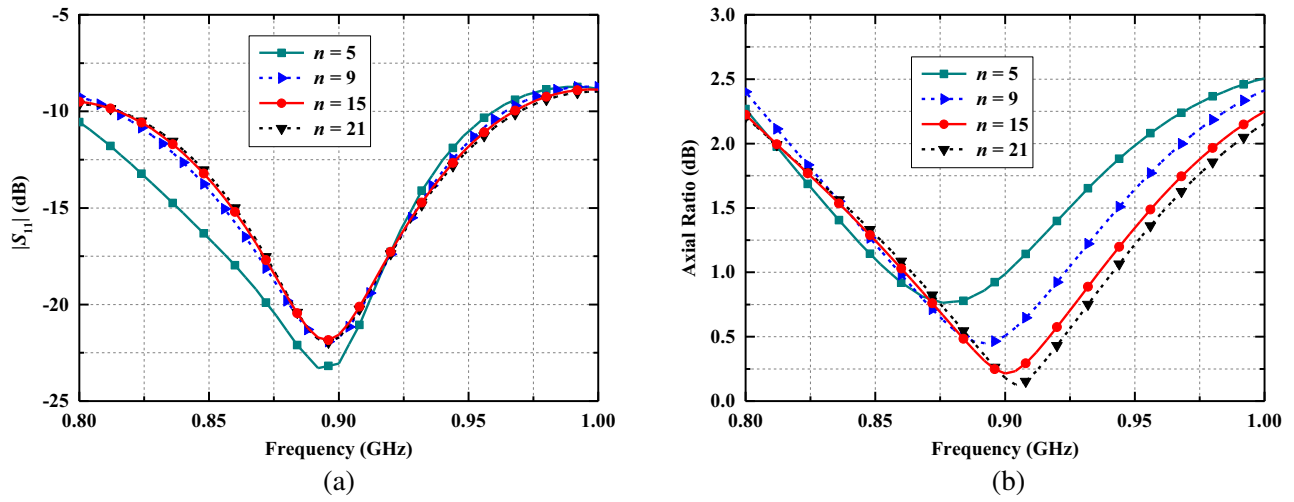


Figure 12. Effect of the number of the shorting pins n on the performances of the proposed CP patch antenna with $(n - 1)D = 105$ mm. (a) $|S_{11}|$. (b) AR.

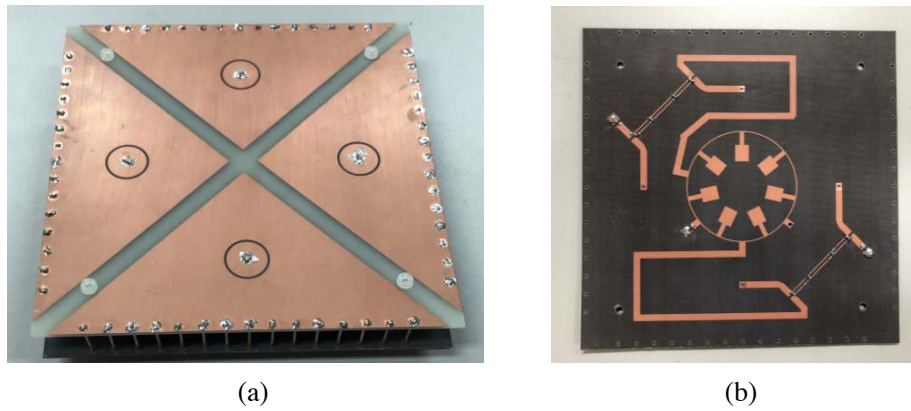


Figure 13. Photograph of the proposed compact broadband CP antenna. (a) Overall view. (b) Feed network.

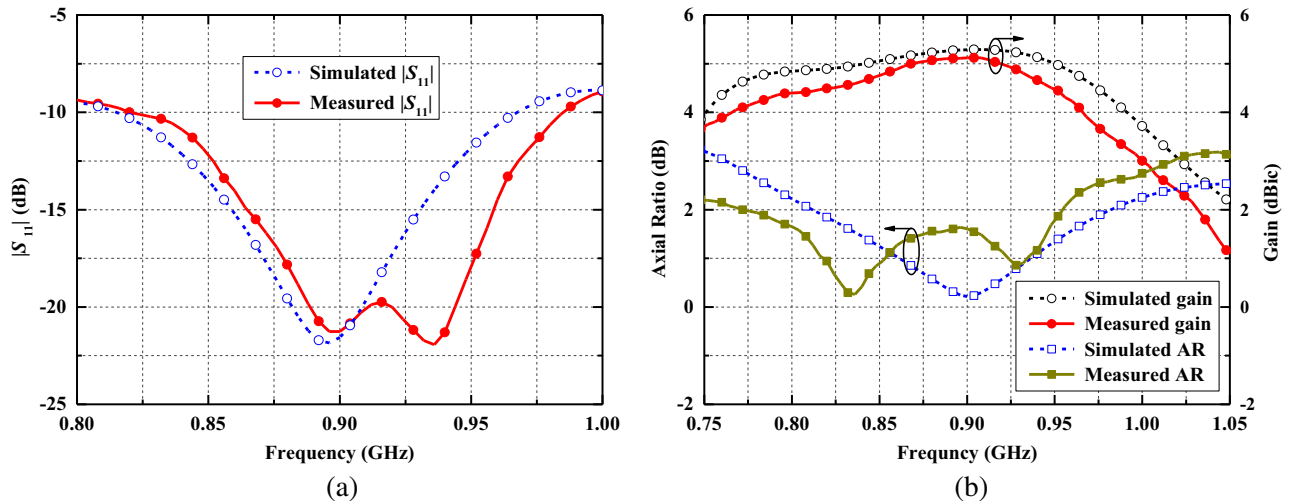


Figure 14. Simulated and measured results of the proposed CP antenna. (a) $|S_{11}|$. (b) AR and gain.

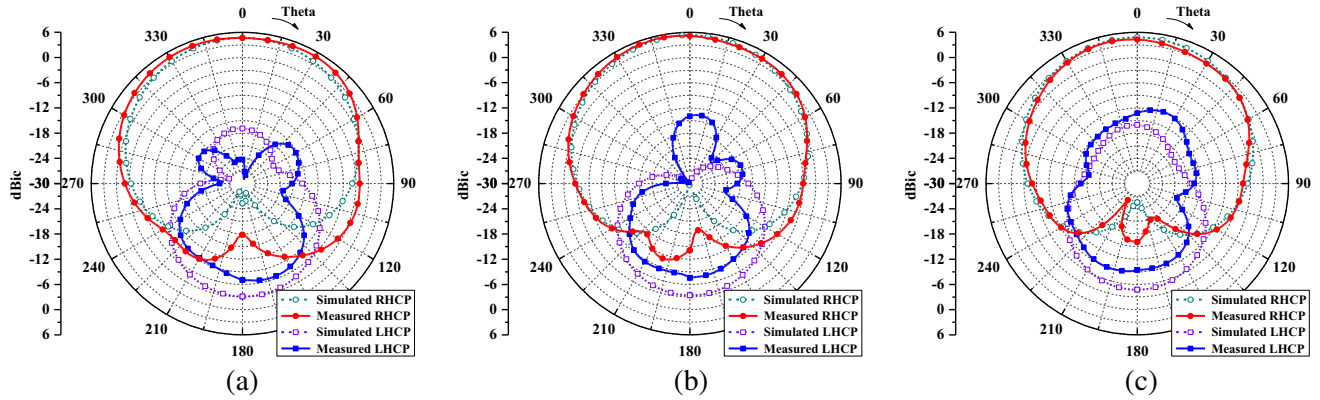


Figure 15. Simulated and measured radiation patterns of the proposed CP antenna. (a) 840 MHz. (b) 900 MHz. (c) 960 MHz.

of the used capacitors and the dielectric constant of the FR4 and F4B substrates in the fabricated prototype.

Figure 15 shows the simulated and measured far-field radiation patterns at 840, 900, and 960 MHz. Symmetrical RHCP radiation patterns in the upper half-space are achieved. The half-power beamwidths for the RHCP at 840, 900, and 960 MHz are 126°, 118°, and 102°, respectively. The simulated and measured 3-dB AR beamwidths of the proposed CP antenna at the center frequency of 900 MHz are shown in Figure 16. It is observed that the measured 3-dB AR beamwidths are 177° and 190° in the planes of $\phi = 0^\circ$ and $\phi = 45^\circ$, respectively. Table 1 compares the proposed CP antenna with the previous UHF RFID patch antennas. The proposed CP antenna provides a wider operation bandwidth (i.e., overlapping bandwidth of impedance matching and 3-dB AR) with wider 3-dB AR beamwidth and half-power beamwidth. The cost of these advantages is the antenna height larger than $0.05\lambda_0$ and a moderate antenna gain.

Table 1. Comparison between the proposed CP antenna and the existing UHF RFID patch antennas.

References	Antenna size	Impedance bandwidth	3-dB AR bandwidth	3-dB AR beamwidth*	Half-power beamwidth#	Gain (dBic)
[2]	$0.75\lambda_0 \times 0.75\lambda_0 \times 0.11\lambda_0$	25.8%	13.5%	76°	64°	8.6
[3]	$0.79\lambda_0 \times 0.79\lambda_0 \times 0.11\lambda_0$	19.7%	11.0%	85°	60°	9.3
[4]	$0.27\lambda_0 \times 0.27\lambda_0 \times 0.014\lambda_0$	1.9%	0.7%	100°	/	3.8
[5]	$0.60\lambda_0 \times 0.60\lambda_0 \times 0.171\lambda_0$	56.5%	6.1%	/	/	7.0
[6]	$0.60\lambda_0 \times 0.60\lambda_0 \times 0.18\lambda_0$	48.6%	16.5%	/	73°	8.6
[7]	$0.45\lambda \times 0.45\lambda_0 \times 0.074\lambda_0$	14.2%	9.0%	/	77°	7.3
[9]	$0.60\lambda_0 \times 0.60\lambda_0 \times 0.089\lambda_0$	21.4%	13.4%	90°	/	7.0
[10]	$0.67\lambda_0 \times 0.67\lambda_0 \times 0.043\lambda_0$	10.6%	6.0%	/	65°	8.9
[11]	$0.75\lambda_0 \times 0.75\lambda_0 \times 0.074\lambda_0$	20.2%	17.7%	90°	/	6.5
[12]	$0.75\lambda_0 \times 0.75\lambda_0 \times 0.075\lambda_0$	13.1%	25.1%	/	/	7.0
[13]	$0.75\lambda_0 \times 0.75\lambda_0 \times 0.11\lambda_0$	25.6%	16.4%	75°	/	8.3
[14]	$0.36\lambda_0 \times 0.36\lambda_0 \times 0.05\lambda_0$	22.7%	4.9%	/	/	5.5
[15]	$0.463\lambda_0 \times 0.463\lambda_0 \times 0.032\lambda_0$	3.5%	0.65%	/	72°	7.2
This work	$0.408\lambda_0 \times 0.408\lambda_0 \times 0.053\lambda_0$	18.4%	> 32.8%*	177°	118°	5.1

* 3-dB AR beamwidth at the center frequency. # Half-power beamwidth at the center frequency.

* AR less than 2.5 dB.

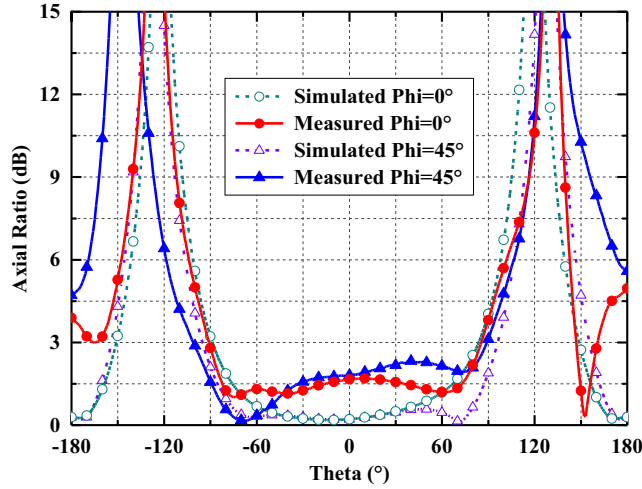


Figure 16. Simulated and measured 3-dB AR beamwidths of the proposed CP antenna.

4. CONCLUSION

In this paper, a compact broadband CP patch antenna has been presented for universal UHF RFID applications. By using shorting pins, the miniaturization of the patch antenna and the enhancement of 3-dB AR beamwidth have been achieved. Besides, T-type transmission-line sections and step-impedance open-circuited stubs have been proposed to further reduce the size of the $7\lambda/6$ ring coupler [23]. Meanwhile, using the advantages of the TRD coupler [22], a compact feed network has been presented for good circular polarization. Compared to the previous broadband UHF RFID patch antennas [2, 3, 5–13], the proposed CP antenna has a wider operation bandwidth with a wider beamwidth and a smaller size.

ACKNOWLEDGMENT

This work was supported by the National Natural Science Foundation of China (Nos. 61871417 and 51809030), the Natural Science Foundation of Liaoning Province (Nos. 2019-MS-024 and 2020-MS-127), the Liaoning Revitalization Talents Program, and the Fundamental Research Funds for the Central Universities (Nos. 3132020206 and 3132020207).

REFERENCES

1. Trinh, L.-H., K.-T. Lu, M.-T. Nguyen, N.-V. Truong, and F. Ferrero, "Miniature circularly polarized antenna for UHF RFID handheld reader: design and experiments," *Progress In Electromagnetics Research M*, Vol. 93, 43–52, 2020.
2. Wang, Z., S. Fang, S. Fu, and S. Jia, "Single-fed broadband circularly polarized stacked patch antenna with horizontally meandered strip for universal UHF RFID applications," *IEEE Trans. Microwave Theory Tech.*, Vol. 59, No. 4, 1066–1073, Apr. 2011.
3. Wang, P., G. Wen, J. Li, Y. Huang, L. Yang, and Q. Zhang, "Wideband circularly polarized UHF RFID reader antenna with high gain and wide axial ratio beamwidths," *Progress In Electromagnetics Research*, Vol. 129, 365–385, 2012.
4. Nasimuddin, Z. N. Chen, and X. Qing, "Asymmetric-circular shaped slotted microstrip antennas for circular polarization and RFID applications," *IEEE Trans. Antennas Propag.*, Vol. 58, No. 12, 3821–3828, Dec. 2010.

5. Sim, C.-Y.-D., C. Lin, T. Chen, J. Liou, and H. Chou, "An eccentric annular slotted patch with parasitic element for UHF RFID reader applications," *IEEE Int. Conf. RFID Technology and Applications*, 37–40, Pisa, Italy, 2019.
6. Sim, C.-Y.-D., Y.-W. Hsu, and G. Yang, "Slits loaded circularly polarized universal UHF RFID reader antenna," *IEEE Antennas Wireless Propag. Lett.*, Vol. 14, 827–830, 2015.
7. Li, J., H. Liu, S. Zhang, M. Luo, Y. Zhang, and S. He, "A wideband single-fed, circularly-polarized patch antenna with enhanced axial ratio bandwidth for UHF RFID reader applications," *IEEE Access*, Vol. 6, 55883–55892, 2018.
8. Pan, Y. M., W. J. Yang, S. Y. Zheng, and P. F. Hu, "Design of wideband circularly polarized antenna using coupled rotated vertical metallic plates," *IEEE Trans. Antennas Propag.*, Vol. 66, No. 1, 42–49, Jan. 2018.
9. Nasimuddin, X. Qing, and Z. N. Chen, "A wideband circularly polarized stacked slotted microstrip patch antenna," *IEEE Antennas Propag. Mag.*, Vol. 55, No. 6, 84–99, Dec. 2013.
10. Chen, X., G. Fu, S.-X. Gong, Y.-L. Yan, and W. Zhao, "Circularly polarized stacked annular-ring microstrip antenna with integrated feeding network for UHF RFID readers," *IEEE Antennas Wireless Propag. Lett.*, Vol. 9, 542–545, 2010.
11. Chung, H. L., X. Qing, and Z. N. Chen, "A broadband circularly polarized stacked probe-fed patch antenna for UHF RFID applications," *Int. J. Antennas Propag.*, Vol. 2007, Art. ID 76793, 8 pages, 2007.
12. Kwa, H. W., X. Qing, and Z. N. Chen, "Broadband single-fed single-patch circularly polarized antenna for UHF RFID applications," *IEEE AP-S Int. Symp.*, 1–4, San Diego, USA, 2008.
13. Chen, Z. N., X. Qing, and H. L. Chung, "A universal UHF RFID reader antenna," *IEEE Trans. Microwave Theory Tech.*, Vol. 57, No. 5, 1275–1282, May 2009.
14. Wu, S., J. Yuan, J. Chen, and Y. Li, "Compact circularly polarized microstrip ring antenna using capacitive coupling structure for RFID readers," *IEEE Access*, Vol. 8, 32617–32623, 2020.
15. Huang, G.-L., C.-Y.-D. Sim, C.-W. Lin, and M.-J. Gao, "Low-profile UHF RFID reader antenna with CP radiation and coupled feeding technique," *Int. J. RF Microw. Comput. Aided Eng.*, Vol. 26, No. 9, 819–828, 2016.
16. Xu, H.-X., G.-M. Wang, J.-G. Liang, M. Q. Qi, and X. Gao, "Compact circularly polarized antennas combining meta-surfaces and strong space-filling meta-resonators," *IEEE Trans. Antennas Propag.*, Vol. 61, No. 7, 3442–3450, Jul. 2013.
17. Xu, H.-X., G.-M. Wang, and M.-Q. Qi, "A miniaturized triple-band metamaterial antenna with radiation pattern selectivity and polarization diversity," *Progress In Electromagnetics Research*, Vol. 137, 275–292, 2013.
18. Xu, H.-X., G.-M. Wang, M. Q. Qi, T. Cai, and T. J. Cui, "Compact dual-band circular polarizer using twisted Hilbert-shaped chiral metamaterial," *Opt. Express*, Vol. 21, No. 21, 24912–24921, Oct. 2013.
19. Ng, K.-B., C. H. Chan, and K. M. Luk, "Low-cost vertical patch antenna with wide axial-ratio beamwidth for handheld satellite communications terminals," *IEEE Trans. Antennas Propag.*, Vol. 63, No. 4, 1417–1424, Apr. 2015.
20. Zhang, X., L. Zhu, and N.-W. Liu, "Pin-loaded circularly-polarized patch antennas with wide 3-dB axial ratio beamwidth," *IEEE Trans. Antennas Propag.*, Vol. 65, No. 2, 521–528, Feb. 2017.
21. Wang, M.-S., X.-Q. Zhu, Y.-X. Guo, and W. Wu, "Compact circularly polarized patch antenna with wide axial-ratio beamwidth," *IEEE Antennas Wireless Propag. Lett.*, Vol. 17, No. 4, 714–718, Apr. 2018.
22. Liu, H., S. Fang, Z. Wang, and T. Shao, "Coupled line trans-directional coupler with improved power distribution and phase performance," *IEEE Int. Symp. Radio-Frequency Integration Technology*, 126–128, Seoul, Korea, 2017.
23. Mandal, M. K. and S. Sanyal, "Reduced-length rat-race couplers," *IEEE Trans. Microwave Theory Tech.*, Vol. 55, No. 12, 2593–2598, Dec. 2007.
24. Pozar, D. M., *Microwave Engineering*, 4th Edition, John Wiley & Sons, New York, 2012.